

# Opposed Jet Flames of Very Lean or Rich Premixed Propane-Air Reactants vs. Hot Products

Zhongxian Cheng\*, Joseph A. Wehrmeyer, and Robert W. Pitz  
Mechanical Engineering Department, Vanderbilt University  
Box 1592 Station B, Nashville, TN 37235

Several opposed jet flames of very lean and rich premixed propane-air versus hot products generated by lean hydrogen flames are investigated in order to study stratified charge combustion processes in a DISI engine. A high spatial resolution visible Raman system is used to measure major species concentration and flame temperature simultaneously. The flames are numerically simulated with the Oppdif/CHEMKIN software using a reduced propane mechanism. Comparisons of the predicted and measured flame structure are made for three flames: rich ( $\phi=1.25$ ) vs. hot products lean ( $\phi=0.64$ ) vs. hot products, and lean ( $\phi=0.60$ ) vs. hot products. The hot products are formed by a hydrogen-air ( $\phi=0.4$ ) flame. A rich premixed  $C_3H_8$ -air ( $\phi=1.25$ ) mixture vs. hot products stream generates a triple flame. The measured flame structure of the rich flame is in good agreement with numerical prediction. Thus the chosen propane mechanism and transport model are at least appropriate for the rich flame. The premixed  $C_3H_8$ -air ( $\phi=0.64$ ) mixture vs. hot products generated a lean premixed self-propagating flame. The  $C_3H_8$ -air ( $\phi=0.60$ ) versus hot products generated a so-called "negative flame speed" flame, which is a diffusion flame formed by reactants diffusing across the stagnation plane and burning in the high temperature lean hot products. In this flame, the predicted and measured  $CO_2$  concentration profiles differ, indicating either the chemical kinetic mechanism or molecular transport model needs further improvement.

## INTRODUCTION

Direct-injection spark-ignition (DISI) engines are changing the automobile power plant situation due to low fuel consumption and high power output [1]. This attractive potential comes from ultra-lean overall stoichiometry. In traditional spark ignition engines, homogeneously premixed reactions occur near stoichiometric conditions. However, in the DISI engine, ultra-lean combustion is achieved by a stratified charge that improves fuel economy in both part load and full load conditions. In part load operation, reduction of pumping work (throttle loss) is the principal contribution to fuel economy. Also contributing, but to a smaller degree is the reduction of wall heat loss and exhaust energy [2]. For full load operation, fuel charge cooling leads to lower temperatures in cylinder and allows a higher compression ratio contributing to improved fuel economy.

The combustion challenges are at low load conditions. Under low load conditions, the fuel is directly injected into the center of the cylinder late in the compression stroke just prior to the spark. The fuel/air mixture is non-homogeneous, leading to the simultaneous formation of stoichiometric, rich and lean flames inside the cylinder. As shown in Fig. 1, the fuel spray can impinge on the cylinder head to form an in-homogeneous region of lean, rich and stoichiometric mixtures. Lean direct injection of hydrocarbon fuel improves engine efficiency but pollutants can be increased. Unburned HC's can be

produced in the lean regions where the flame is so lean that the flame is extinguished and the fuel is not completely consumed. In the stoichiometric regions excess NO is formed; and in the rich regions soot can be produced.

The opposed jet burner generates ideal counterflow flames that are widely used to study chemical kinetics and species transport under aerodynamic stretch. For example, gas sampling, thermocouple and LDV were used to measure the species concentration, flame temperature, and axial velocities for partially premixed counterflow flames [3]. Ultraviolet laser-induced Raman scattering was used to study hydrogen-air diffusion flames from a counterflow burner [4,5] and partially premixed methane-air versus air flame structure was investigated [6]. Major species (reactants and products) concentration and temperature can be determined for experiments with calibration procedures.

The purpose of the present study is to understand partially premixed very lean or rich flames in a counter flow geometry in order to improve fuel consumption and to reduce the pollutants from these flames. In particular, how hot products can support the burning of very lean or rich flames is studied. These partially premixed flames are modeled by a stream of opposed jets as shown in Fig. 2. There has been little experimental work done on flame structure for partially premixed flames of hot products vs. very lean or rich mixtures. These planar opposed jet flames are representatives of the types of flames found in DISI

\* Corresponding author: zhongxian.cheng@vanderbilt.edu

Proceeding of the 2002 Technical Meeting of the Central States Section of The Combustion Institute

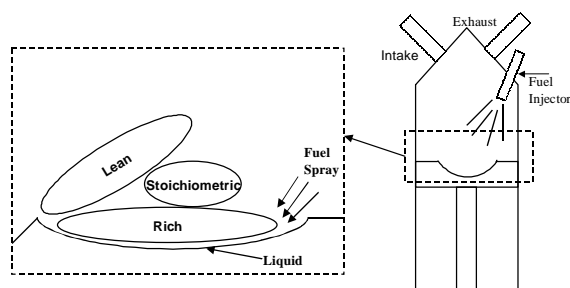


Figure 1. Schematic of stratified charge operation in DISI engine.

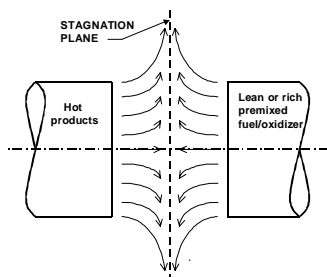


Figure 2. Opposed jet flame schematic: hot products vs. lean or rich reactants.

engine. The experimental results are compared to numerical predictions obtained from Oppdif, part of the CHEMKIN Collection.

## EXPERIMENTS

Figure 3 shows a schematic of the laser system. The 532 nm Nd:YAG laser beams are stretched with a beam splitter, passed through a zero order polarization rotator (not shown) and focused by a 0.3 m lens. Two Stanford Research Systems DG535 pulse generators synchronize all the trigger signals for all devices in the system. The Raman light collecting system consists of a f/1.5 Cassegrain optics and 0.65 m spectrometer (SPEX 1800, 0.75-meter Czerny Tuner Spectrometer, modified to 0.65 m). The measuring sample is a cylinder (length is 4.7 mm and diameter is 0.2 mm). For the planar flame measurement, the 0.2 mm dimension is transverse to the concentration gradient. Thus, the 0.2 mm dimension is the spatial resolution of the system. The Raman scattered light is collected by the Cassegrain lens and passed through a ferroelectric shutter, a mechanical shutter, and an entrance slit to the 0.65 m spectrometer. The 0.65 m spectrometer has a 600 groove/mm grating, giving a final dispersion of 0.39 mm/nm. A mechanical shutter (DISPLAYTEC, DR50 FLC Driver) is used as an external shutter for the liquid nitrogen cooled CCD camera but has a relatively long exposure time (6 ms). A ferroelectric shutter is placed in front of the mechanical shutter to cut off flame luminosity into the spectrometer by its short exposure time (30  $\mu$ s).

A liquid nitrogen cooled charge coupled device (LN/CCD) is used to obtain Raman spectra. An orange Schott glass filter is placed in front of the LN/CCD to block any stray 532 nm lights. A separate long pass filter (Dielectric Short Wave Pass Filter, 750 nm cutoff) eliminates the infrared radiation from the flame. The LN/CCD is synchronized with other devices and delivers collecting data to computers. The LN/CCD camera has a 1024 x 1024 pixel chip, mounted to the back plane of the spectrometer and aligned in wavelength dimension and the spatial dimension. The chip is back-illuminated to give high quantum efficiency in the visible. The sample volume length is limited by the entrance slit image and is about 4.7 mm. The minimum imaging spatial resolution of the system is experimentally determined by a Ronchi grating to be about 50  $\mu$ m. The planar flame composition did not vary along the 4.7 mm beam length and the 1024 pixels along the spatial dimensions were binned into one super pixel. In wavelength dimension, resolution is  $\sim$ 17 pixels/nm.

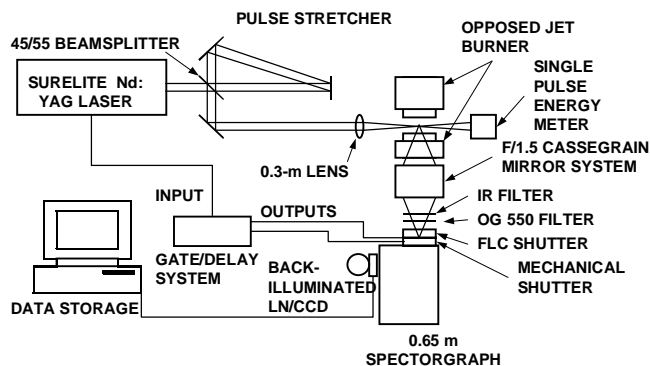


Figure 3. Lasersystem schematic

A translation stage equipped with a motion control unit is controlled via a LabVIEW interface and can move the burner in the horizontal and vertical directions automatically. The opposed jet burner used for this work was described in detail in reference [7] and it was modified from the design by Seshadri [4]. It consists of two 25 mm diameter straight jets which are separated by 12.5 mm. For each jet, there are 5 pieces of fine (100#) mesh screens inside the jet to keep the flow uniform. Glass beads (6 mm diameter) are filled in the bottom jet under of mesh screen to prevent flame flashback. For this work, premixed  $C_3H_8$ -air flows into the bottom jet and premixed  $H_2$ -air mixture flows into the top jet. If the momentums of the two flows are balanced, a stagnation plane exists between the two jets. For the bottom jet, co-flow nitrogen shields the flame and prevents outside air going into flame. At the same time, this limits the annular boundary of the flames and prevents the flame from extending to far outside of jet. The hot waste gas is sucked into an annular exhaust section on the top jet and it is cooled by a jacket water system. The suction exhaust is connected to a ventilated hood.

## FLAMES EXAMINED

As mentioned earlier, DISI engines under low load produce stratified combustion. Pollutants can be formed in very lean or rich regions. The presence of hot products can improve combustion in these regions. In this work we study how hot products support either very rich or very lean combustion by using an opposed jet flame as a model. Three opposed jet flames are selected to simulate these situations. Each of them has a jet of lean hydrogen-air premixed reactants impinging upon a jet of premixed propane-air reactants. Propane is chosen because propane is a relatively simple hydrocarbon fuel, and its chemical burning characteristics more closely represent real fuels, such as gasoline. In addition, propane is gaseous fuel at regular pressure and its detailed chemical kinetic mechanism has been investigated [8]. High temperature water vapor and CO<sub>2</sub> are the major products of stoichiometric reaction. For convenience, hot products from a lean hydrogen-air premixed flame are chosen to simulate hot products that impinge on the lean or rich premixed reactants. This choice is based on the fact that the premixed hydrogen flame has a fast laminar flame speed relative to the premixed hydrocarbon-air flame. Therefore the effect of strain rate on propane-air flames can be studied individually, without considering the influence of strain rate on hydrogen-air flames. Another advantage is that no carbon exists in the H<sub>2</sub>-air flame products and thus, all the carbon-bearing products (i.e., CO<sub>2</sub> or CO) come from the propane-air premixed flames. Thus one can easily see if the hot products lead to the additional burning of the HC fuel.

The axial strain rate  $a$  of counterflow flames is given by Kim et al. [9]

$$a = \frac{2V_O}{L} \left( 1 + \frac{V_F \sqrt{\rho_F}}{V_O \sqrt{\rho_O}} \right)$$

where  $V$  is the jet exit velocity,  $\rho$  is the gas density,  $L$  is the jet separation and subscripts  $F$  and  $O$  denote the two jets, respectively. The counterflow flame at high flow rates can cross the stagnation plane into the hot products side to form so-called “negative flame speed” flame [10]. The definition of “negative flame speed” stemmed from the original definition of laminar flame velocity that is opposite of the convective velocity at the front edge of the preheat zone of a planar one-dimensional flame. Normally, the bulk convective motion directs the fresh unburned mixture through flame zone to form burned products.

## REACTION MECHANISM

The chemical kinetic mechanism, called M5 propane mechanism by Haworth et al. [8] was used for the numerical simulation. It was modified from Warnatz’s [11] base propane-air mechanism. The M5 reaction mechanism has 73 reactions and 39 species. The mechanism eliminates reactions involving n-C<sub>3</sub>H<sub>7</sub> and

modifies rate coefficient in the reaction that converts i-C<sub>3</sub>H<sub>7</sub> to C<sub>3</sub>H<sub>6</sub> and makes fuel breakdown steps irreversible. These changes improve computation speed while maintaining reasonable accuracy over a broad range of reactant stoichiometry [8].

## RESULTS AND DISCUSSION

### (1) Rich C<sub>3</sub>H<sub>8</sub> flame versus hot products

Experimental measurements and numerical predictions of temperatures and reactant concentrations are compared in Fig. 4. To facilitate comparison of the widths and peak values for the experimental and numerical profiles, the numerical data and stagnation plane location have been shifted toward the C<sub>3</sub>H<sub>8</sub>-air side by 0.5 mm. This small discrepancy in location could be because of errors in initial positioning of the laser with respect to the bottom nozzle location and/or to partial burning of the H<sub>2</sub>-air jet in the nozzle (describe below) which would increase the momentum flux exiting that nozzle. It is found that experimental profiles of O<sub>2</sub>, N<sub>2</sub> and C<sub>3</sub>H<sub>8</sub> match with numerical profiles in most regions. In the rich premixed C<sub>3</sub>H<sub>8</sub> flame zone, O<sub>2</sub> concentration drops to zero theoretically but some experimental data points deviate from zero, having value of 2~3% in mole fraction. However, the general trend in the O<sub>2</sub> profiles is similar. The deviations could be caused by the overlap of the O<sub>2</sub> and CO<sub>2</sub> Raman lines that was not properly corrected in the calibration procedure. Fig. 5 shows experimental measurement and numerical prediction of product concentrations. The CO peak concentration (8.5%) and the peak CO location from experimental data agree with the prediction. But the experimental CO profile is wider than the predicted profile. There is an opposite discrepancy for the CO<sub>2</sub> profile where the numerically predicted profile is wider than experimental results.

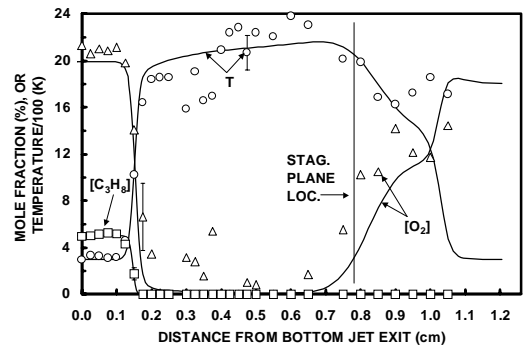


Figure 4. Experimental and numerically-predicted reactant profiles for a partially-premixed opposed jet flame. C<sub>3</sub>H<sub>8</sub>-air ( $\phi=1.25$ ) vs. H<sub>2</sub>-air ( $\phi=0.4$ ). Experimental strain rate = 180 sec<sup>-1</sup>. Numerical data shifted by 0.5 mm.

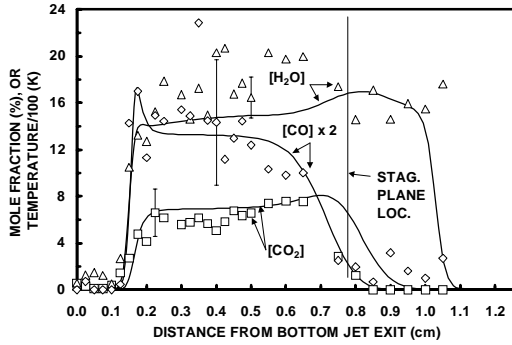


Figure 5. Experimental and numerically-predicted reactant profiles for a partially-premixed opposed jet flame.  $C_3H_8$ -air ( $\phi=1.25$ ) vs.  $H_2$ -air ( $\phi=0.4$ ). Experimental strain rate =  $180 \text{ sec}^{-1}$ . Numerical data shifted by 0.5 mm.

## (2) Lean, “positive flame speed” $C_3H_8$ flame versus hot products

Figures 6 and 7 show the reduced experimental data and related numerical predictions for the lean “positive flame speed” flame. Based on numerical predictions, the lean premixed  $H_2$ -air flame is located away from top jet. However, the experimental data shows the  $H_2$ -air flame is anchored near the nozzle exit, where temperature and water vapor concentration are experimentally measured at high values. This anchoring is probably caused by the retaining ring that is located near exit of the nozzle to keep the screen mounted inside top jet. This causes the lean  $H_2$ -air flame to attach at the exit of nozzle. As seen from experimental data, a premixed “positive flame speed” flame exists. The experimental  $CO_2$  profile has a  $\sim 8\%$  peak value and experimental  $O_2$  has a  $\sim 7\%$  minimum value, which is obviously lower than the  $\sim 12\%$  value on the side of  $H_2$ -air jet where there is excess  $O_2$  after combustion.

From Figs. 6 and 7, it is found that numerical predictions give similar trends as the experimental results in the premixed flame zones. The experimental  $O_2$ ,  $C_3H_8$ ,  $H_2O$ , and  $CO_2$  profiles agree well with numerical prediction in both the premixed flame zone and the diffusion zone. But near the hot products side, there is a deviation for  $H_2O$  profile between the experimental result and the numerical prediction. The reason is that  $H_2$ -air flame is actually anchored near nozzle exit. In the premixed flame zone, the radiation heat loss could cause the difference in temperature profile.

In order to simulate the anchoring of the  $H_2$ -air flame seen in the actual experiment, hot products boundary conditions (high temperature  $H_2O$  and high velocity of products) are used instead of cold reactants. A hot products boundary condition assumes that lean  $H_2$ -air mixture is completely burned inside the top jet nozzle. Under these conditions, the related temperature and  $H_2O$  concentration are estimated by an adiabatic equilibrium calculation. The hot products velocity can be estimated by the ideal gas law.

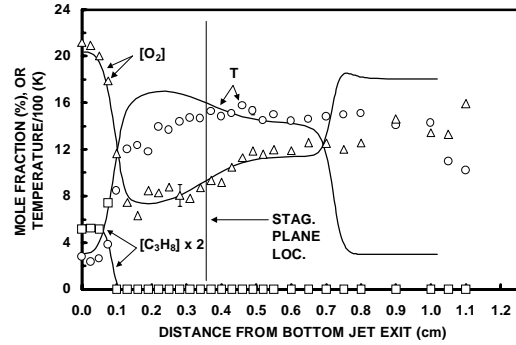


Figure 6. Experimental and numerically-predicted reactant profiles for a partially-premixed opposed jet flame.  $C_3H_8$ -air ( $\phi=0.64$ ) vs.  $H_2$ -air ( $\phi=0.4$ ). Experimental strain rate =  $140 \text{ sec}^{-1}$ . Numerical data shifted by 2.4 mm.

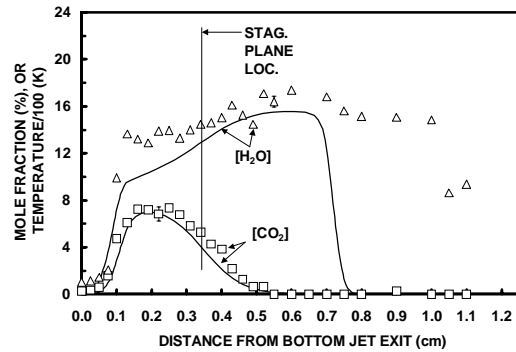


Figure 7. Experimental and numerically-predicted reactant profiles for a partially-premixed opposed jet flame.  $C_3H_8$ -air ( $\phi=0.64$ ) vs.  $H_2$ -air ( $\phi=0.4$ ). Experimental strain rate =  $140 \text{ sec}^{-1}$ . Numerical data shifted by 2.4 mm.

Under the assumption of complete burning of the  $H_2$ -air mixture inside the nozzle, the hot product velocity increases from  $47 \text{ cm/s}$  to  $205 \text{ cm/s}$ . Figs. 8 and 9 show the numerical results with this hot products boundary condition.

In Fig. 8, the numerical results predict that the previous premixed “positive flame speed” flame shown in Fig. 6 doesn’t exist on the  $C_3H_8$ -air side of stagnation plane. Instead, the lean  $C_3H_8$  mixture diffuses into the hot products side and forms a weak diffusion flame (so-called “negative flame speed” flame) that is supported by the high temperature of hot products. This type of flame has been predicted by Darabiha et al. [12] at high strain rates in lean premixed vs. hot products opposed jet flames. In Fig. 9, the numerically predicted peak  $CO_2$  concentration is very low compared to that shown in Fig. 7. The predicted  $CO_2$  level is almost two orders of magnitude lower than the measured results shown in Fig. 9. The experimentally observed existence of the premixed  $C_3H_8$ -air flame on the left side of the stagnation plane indicates that using adiabatic

combustion hot products as boundary condition for the numerical prediction is unreasonable. The real boundary conditions should be that a partial degree of reaction occurs for  $H_2$ -air reactants inside the jet. Unfortunately, the velocity at the  $H_2$ -air jet exit was not measured to determine the degree of partial burning.

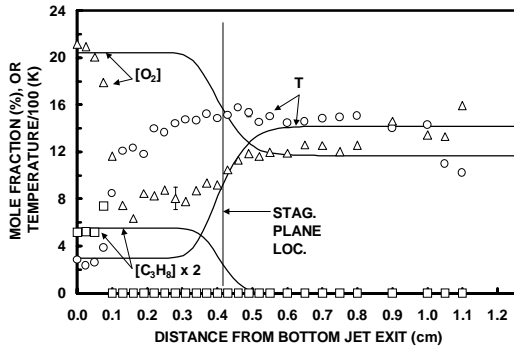


Figure 8. Experimental and numerically-predicted reactant profiles for a partially-premixed opposed jet flame.  $C_3H_8$ -air ( $\phi=0.64$ ) vs.  $H_2$ -air ( $\phi=0.4$ ). Experimental strain rate =  $390 \text{ sec}^{-1}$ . Numerical boundary conditions and experimental strain rate assume  $H_2$ -air reacts in nozzle. Experimental data same as in Figure 6.

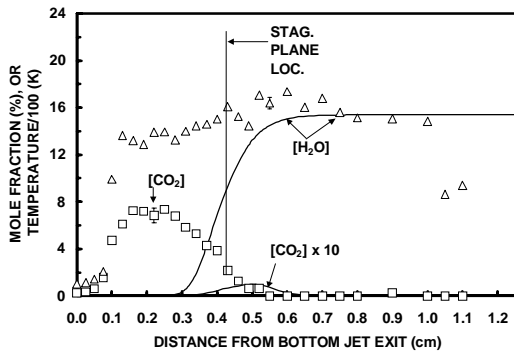


Figure 9. Experimental and numerically-predicted reactant profiles for a partially-premixed opposed jet flame.  $C_3H_8$ -air ( $\phi=0.64$ ) vs.  $H_2$ -air ( $\phi=0.4$ ). Experimental strain rate =  $390 \text{ sec}^{-1}$ . Numerical boundary conditions and experimental strain rate assume  $H_2$ -air reacts in nozzle. Experimental data same as in Figure 7.

### (3) Very lean, “negative flame speed” $C_3H_8$ flame versus hot products

Figures 10 and 11 show the experimental results and numerical predictions with equilibrium hot products as the boundary condition (complete burning of the  $H_2$ -air mixture inside the nozzle) for a lean  $C_3H_8$ -air ( $\phi=0.60$ ) mixture impinging upon an  $H_2$ -air jet ( $\phi=0.4$ ). There is only a slight difference for this premixed mixture compared to the previous “positive flame speed” flame: the equivalence ratio is decreased from 0.64 to 0.6. It indicates a lean  $C_3H_8$ -air premixed “positive flame speed” flame doesn’t exist on the

$C_3H_8$ -air side of the stagnation plane. The  $C_3H_8$  Raman signal disappears around stagnation plane, indicating that either the  $C_3H_8$  fuel reacts in this zone or  $C_3H_8$  is convected away at the stagnation plane. In fact, it is found there is a very weak flame which is formed by  $C_3H_8$  diffusing across the stagnation plane and reacting with the excess  $O_2$  from the  $H_2$ -air premixed flame from the top jet. This weak flame is called a “negative flame speed” flame [10,12]. This flame is so weak that it can only be seen by eye in a dark room. Normal exposure 35 mm camera pictures were taken in the darkened room but the flame did not appear on the photographs. There are two prerequisites for this weak flame existing: 1) high strain rate and 2) excess oxidizer and high temperature hot products from the top jet to support it.

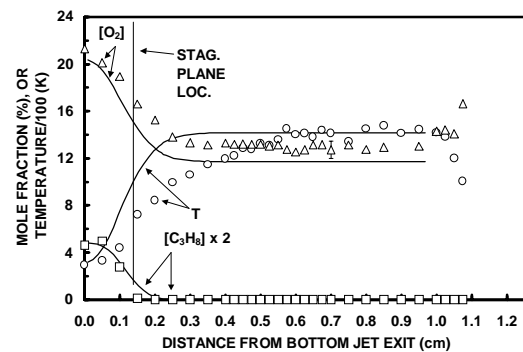


Figure 10. Experimental and numerically-predicted reactant profiles for a partially-premixed opposed jet flame.  $C_3H_8$ -air ( $\phi=0.60$ ) vs.  $H_2$ -air ( $\phi=0.4$ ). Experimental strain rate =  $390 \text{ sec}^{-1}$ . Numerical boundary conditions and experimental strain rate assume  $H_2$ -air reacts in nozzle. Numerical data shifted by 2.9 mm.

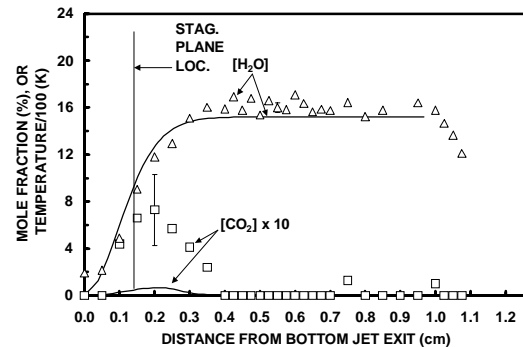


Figure 11. Experimental and numerically-predicted reactant profiles for a partially-premixed opposed jet flame.  $C_3H_8$ -air ( $\phi=0.60$ ) vs.  $H_2$ -air ( $\phi=0.4$ ). Experimental strain rate =  $390 \text{ sec}^{-1}$ . Numerical boundary conditions and experimental strain rate assume  $H_2$ -air reacts in nozzle. Numerical data shifted by 2.9 mm.

The concentration of  $CO_2$  peak is about 0.06%, far lower than experimental result 0.7%. It is reported that the peak value of the  $CO_2$  profile and location is sensitive to boundary velocity for a negative flame [12]. The peak value

of CO<sub>2</sub> drops and its location is closer to the stagnation plane with increasing strain rate. Reactant and temperature profiles will steepen across the diffusion zone as strain rate increases. However, a prediction (not shown) with boundary conditions of cold reactants (47 cm/s velocity and room temperature) instead of completely burned products still shows CO<sub>2</sub> (0.2 %) concentration lower than experimental result (0.7 %). Thus with both boundary conditions, a consistent discrepancy between peak CO<sub>2</sub> experimental and numerical values is found for this very lean flame. This suggests that lean, strained and low temperature C<sub>3</sub>H<sub>8</sub>-air combustion process is not adequately modeled by the chemical reaction mechanism and/or transport data. Improved modeling of the diffusive transport process is especially necessary for the lean “negative flame speed” flame whose reaction rate is controlled by diffusion.

## CONCLUSIONS

An investigation of the flame structure of very lean and rich partially premixed flames versus hot products has been made. Three typical propane-air flames are studied by experiment and numerical simulation. The understanding of these flame structures further helps reduce unburned fuel and the pollutants from these flames. Among these flames, a triple flame of rich premixed C<sub>3</sub>H<sub>8</sub>-air ( $\phi=1.25$ ) impinging hot products has good agreement between experiment data and numerical results.

For a “positive flame speed” flame of lean C<sub>3</sub>H<sub>8</sub>-air ( $\phi=0.64$ ) mixture impinging on hot products, discrepancies between numerical results and experimental data exist for the flame location, thus the numerical data are shifted toward the C<sub>3</sub>H<sub>8</sub>-air side to give a better comparison. Boundary conditions (velocity and temperature) in the hot product side have a significant influence on premixed flame location and concentration of products.

For a “negative flame speed” flame of lean C<sub>3</sub>H<sub>8</sub>-air ( $\phi=0.60$ ) impinging upon hot products, experimental data and numerical prediction give the same result: a very weak diffusion flame locates on the hot products side. The predicted CO<sub>2</sub> concentration is almost an order of magnitude less in peak value than for experimental profile using hot products as boundary conditions. So it may be concluded that some improvements are necessary for the chemical kinetics mechanism model or the molecular transport model to simulate C<sub>3</sub>H<sub>8</sub> “negative flame speed” flames.

## ACKNOWLEDGEMENTS

The authors would like to acknowledge U.S. Department of Energy’s Office of Basic Energy Sciences who have supported this work through a Partnerships for Academic-

Industrial Research (PAIR) grant (No. DE-FG02-98ER14915, with Dr. Alan H. Laufer as the technical monitor).

## REFERENCES

1. Takagi, Y. (1998), “A New Era in Spark-Ignition Engines Featuring High-Pressure Direct Injection,” *Proceedings of the Combustion Institute* **27**, pp. 2055-2068.
2. Zhao, F., Lai, M. -C., and Harrington, D. L. (1999), “Automotive Spark-Ignited Direct-Injection Gasoline Engines,” *Progress in Energy and Combustion Science* **25**, pp. 437-562.
3. Smooke, M. D., Seshadri, K. and Puri, I. K. (1988), “The Structure and Extinction of Partially Premixed Flames Burning Methane in Air,” *Proceedings of the Combustion Institute* **22**, pp. 1555-1563.
4. Trees, D., Brown, T. M., Seshadri, K., Smooke, M. D., Balakrishnan, G., Pitz, R. W., Giovangigli, V., and Nandula, S. P. (1995), “The Structure of Nonpremixed Hydrogen-Air Flames,” *Combustion Science and Technology* **104**, pp. 427-439.
5. Brown, T. M., Tanoff, M. A., Osborne, R. J., Pitz, R. W., and Smooke, M. D. (1997), “Experimental and Numerical Investigation of Laminar Hydrogen-Air Counterflow Diffusion Flames,” *Combustion Science and Technology* **129**, pp. 71-88.
6. Tanoff, M. A., and Smooke, M. D., Osborne, R. J., Brown, T. M., Pitz, R. W., (1996), “The Sensitive Structure of Partially Premixed Methane-Air vs. Air Counterflow Flames,” *Proceedings of the Combustion Institute* **26**, pp. 1121-1128.
7. Osborne, Robin J. (1999), “Application of Ultraviolet Raman Spectroscopy to Methane-Air vs. Air Counterflow Flames,” Master Thesis, Vanderbilt University.
8. Haworth, D. C., Blint, R. J., Cuenot, B., and Poinot, T. J. (2000), “Numerical Simulation of Turbulent Propane-Air Combustion with Nonhomogeneous Reactants,” *Combustion and Flame* **121**, pp. 395-417.
9. Kim, J. S., Libby, P. A., and Williams F. A. (1992), “On the Displacement Effects of Laminar Flames,” *Combustion Science and Technology* **87**, pp. 1-25.
10. Sohrab, S. H., Ye, Z. Y., and Law, C. K. (1984), “An Experimental Investigation on Flame Interaction and the Existence of Negative Flame Speeds,” *Proceedings of the Combustion Institute* **20**, pp. 1957-1965.
11. Warnatz, J. (1981), “The Structure of Laminar Alkane-, Alkene-, and Acetylene Flames,” *Proceedings of the Combustion Institute* **18**, pp. 369-384.
12. Darabiha, N., Candel, S. M., and Marble, F. E. (1986), “The Effect of Strain Rate on a Premixed Laminar Flame,” *Combustion and Flame* **64**, pp. 203-217.